Title

Intracellular pH measurements made simple by fluorescent protein probes and the phasor approach to fluorescence lifetime imaging

Journal

Chemical Communications, 48(42)

ISSN

1359-7345

Authors

Battisti, Antonella
Digman, Michelle A
Gratton, Enrico
et al.

Publication Date

2012

DOI

10.1039/c2cc30373f

Published in final edited form as:
Chem Commun (Camb). 2012 May 25; 48(42): 5127–5129. doi:10.1039/c2cc30373f.

Intracellular pH measurements made simple by fluorescent protein probes and the phasor approach to fluorescence lifetime imaging†

Antonella Battisti[a], **Michelle A. Digman**[b], **Enrico Gratton**[b], **Barbara Storti**[a], **Fabio Beltram**[a], and **Ranieri Bizzarriz**[‡,a]

Antonella Battisti: antonella.battisti@sns.it; Ranieri Bizzarriz: r.bizzarri@sns.it

[a]NEST, Scuola Normale Superiore and Istituto Nanoscienze-CNR, Piazza San Silvestro 12, 56127 Pisa, Italy., Fax: +39 050509417; Tel: +39 05050976

[b]Laboratory for Fluorescence Dynamics, University of California, Irvine, USA

Abstract

A versatile pH-dependent fluorescent protein was applied to intracellular pH measurements by means of the phasor approach to fluorescence lifetime imaging. By this fit-less method we obtain intracellular pH maps under resting or altered physiological conditions by single-photon confocal or two-photon microscopy.

Intracellular pH (pH_i) is a fundamental modulator of cell function, being related to metabolism and growth,[1] ion transport and homeostasis,[2] endocytosis,[3] muscle cellular contractility,[4] apoptosis and cancer,[5] impairment of posttranslational modifications of secreted proteins,[6] neuronal excitability, cell–cell coupling, and signal cascades.[7]

Thanks to pH-sensitive chromophores, fluorescence microscopy can yield high-resolution spatio-temporal pH_i maps in living cells with minimal invasiveness.[8] In this context pH-sensitive mutants of the Green Fluorescent Protein from *Aequorea Victoria* jellyfish (collectively named AFPs) are probably the most attractive pH_i probes available.[9] Indeed, these indicators can be expressed in cells, tissues, and whole organisms as fusion chimeras with specific protein motifs that target them to subcellular compartments characterized by interesting pH_i homeostasis.[10] Furthermore, AFP-fusion proteins seldom cause (photo)toxicity. The peculiar optical pH-sensitivity displayed by many AFPs arises from the proton ionization equilibrium of the phenol group in the chromophore (see Chart 1). Owing to large changes in electron density and resonance,[11] the absorption of the deprotonated chromophore is significantly red-shifted compared to the protonated chromophore form (Chart 1). The emission wavelengths of the two forms are more similar (Chart 1), because the neutral chromophore usually undergoes excited state proton transfer to yield an excited state with anionic structure.[12]

The most effective AFP-based pH_i indicators reported insofar are ratiometric: the pH value in each pixel is the ratio of the fluorescence intensities collected in two suitable emission

†Electronic supplementary information (ESI) available: (1) Materials and methods, (2) theory of phasor dependence on pH, (3) fitting of lifetime decays for calibration solutions with Fig. S1, (4) comparison between FLIM images collected at 740 and 800 nm by TPE (Fig. S2).

Correspondence to: Antonella Battisti, antonella.battisti@sns.it; Ranieri Bizzarriz, r.bizzarri@sns.it.

‡Present Address: Istituto di Biofisica-CNR, *via* Moruzzi 1 - 56124, Pisa, Italy.

intervals, or of the intensities following excitation at two specific wavelengths; this ratio is independent of the indicator's intracellular concentration.[10] Ratiometric pH indicators display multiple excitation–emission maxima with opposite pH dependence. Yet, well-known drawbacks of ratiometry are the reduction of the signal-to-noise ratio at low intensities, owing to the intrinsic error amplification of the ratio operation, and the wavelength-dependent focal depth in wide-field microscopy.

Fluorescence lifetime imaging (FLIM) is an excellent alternative to ratiometric measurements, since fluorescence lifetime is concentration independent and a single excitation wavelength/emission interval is required.[13] In some pH-dependent AFPs, the two protonation states of the chromophore display fairly different lifetimes, making these probes suitable for FLIM-based pH_i measurement.[14] The major drawback of conventional FLIM, however, is the small number of photons usually collected per pixel (~ 500–1000). This is barely enough to distinguish a single from a double exponential decay, which represents the minimum requirement to determine if at least two species are present in the same pixel. Also, AFPs usually display multi-exponential decays for each pH state, making the emission decay analysis at each pixel a demanding computational problem.

The *phasor analysis,* developed by Jameson, Gratton, and Hall,[15] was shown to overcome the main drawbacks of FLIM measurements in several contexts.[16,17] In short, phasor analysis uses a graphical approach to determine the relative ratio of two molecular species by representing in a polar 2D plot (*phasor plot* or *A/B plot*[18]) the cosine ($g_{i,j}$) and sine ($s_{i,j}$) Fourier transforms of the normalized emission decay collected in each pixel *i, j*. For monoexponential decays, the phasor ($g_{i,j}$, s_{ij}) lies on a semicircle (*universal circle*) of radius 1/2 and center (1/2,0); for multi-exponential decays the phasor lies inside the semicircle. Any two-state mixture must give a phasor lying on the segment connecting the phasors of the two individual states, regardless of the number of exponentials they entail (ESI[†]).[16,18,19] The relative distance of the mixture's phasor from the individual states reflects the fractional intensity contribution of each state. From this the molar fractions of the mixture can be inferred.[16,18,19]

In this work, we apply phasor analysis to FLIM-based pH_i measurements using an AFP indicator carefully tailored to monitor pH_i (E^2GFP: F64L/S65T/T203Y GFP).[20] We show that this approach leads to a fast graphical determination of pH_i maps under different physiological conditions, requiring only a preliminary phasor calibration in the pH working range of the fluorescent indicator. Also, we demonstrate that autofluorescence can be easily distinguished from indicator emission, since autofluorescence phasors fall clearly outside the segment accounting for all pH values measurable by the indicator. This improves pH_i detection accuracy.

Although E^2GFP is characterized by multiple proton exchanges involving the chromophore, the protein optical properties follow a single protonation equilibrium with $pK_a = 6.78$ both *in vitro* and in cells.[21] The low-pH state of E^2GFP emits at 510 nm and possesses $\Phi = 0.10$; its high-pH counterpart emits at 525 nm and is significantly brighter as $\Phi = 0.88$.[9] The two states are characterized by different emission time decays. The decay of the high pH-state is almost mono-exponential with $\tau = 3.49$ ns; conversely, at low-pH the decay is a triple-exponential with $\tau_1 = 3.49$ ns, $\tau_2 = 1.13$ ns, and $\tau_3 = 0.49$ ns (Fig. 1a). Excitation at 405 nm affords comparable global emission intensity in the 500–600 nm range, thus representing the

[†]Electronic supplementary information (ESI) available: (1) Materials and methods, (2) theory of phasor dependence on pH, (3) fitting of lifetime decays for calibration solutions with Fig. S1, (4) comparison between FLIM images collected at 740 and 800 nm by TPE (Fig. S2).

best option for accurate detection of pH-associated lifetime changes. A similar photophysical behavior is observed by two-photon excitation (TPE) at 800 nm.

We obtained a universal pH calibration of E^2GFP on the phasor plot. The calibration provides the correspondence between a phasor ($g_{i,j}$, $s_{i,j}$) and the pH measured in that pixel in target cell samples according to the Henderson–Hasselbalch equation (see theoretical description in ESI†). Calibration measurements were collected by single-photon excitation (SPE) at 405 nm on pH-clamped E^2GFP-expressing cells or by TPE at 800 nm in buffer solutions of E^2GFP. As expected (eqn S4a and b in ESI†), phasor plots show good linear arrangements of pixel clusters corresponding to each pH value, with the highest pH phasors lying very close to the universal circle, according to the mono-exponential decay behavior at high pH (Fig. 1b). The linear arrangement of pixel clusters excludes the presence of FRET between protonated and anionic states of E^2GFP in protein dimers that may occur at the intracellular level. We should also add that the presence of dimers at the typical intracellular protein concentrations adopted in the experiment has been excluded by dynamic anisotropy measurements (not shown).

Note that the pixel clusters collected by TPE are displaced with respect to SPE phasors, owing to the different repetition rate of the two exciting sources (405 nm: 40 MHz, 800 nm: 80 MHz). Additionally, SPE measurements were characterized by a higher signal-to-noise ratio than TPE, as shown by the narrower pixel distribution in the phasor plot. This effect may be attributed to lower brightness of E^2GFP under the adopted TPE conditions. As predicted from theory (eqn S6a and b, ESI†), plots of $g_{i,j}$ and $s_{i,j}$ *vs.* pH were adequately fitted to the Henderson–Hasselbalch equation yielding $pK_a = 6.85$ (Fig. 1c), in excellent agreement with the thermodynamic pK_a of E^2GFP.[21] The same pH dependence was also observed on τ_{av} obtained by multi-exponential fitting of lifetime decays collected for calibration solutions (Fig. S1, ESI†). This further confirms the physical equivalence between the phasor approach and conventional FLIM. The accuracy of pH determination was estimated by inspecting cells clamped to the same pH: we found out that accuracy is slightly pH dependent as the standard deviations are $\sigma = 0.015$ pH unit at pH = 6.0, $\sigma = 0.08$ pH unit at pH = 7.2, and $\sigma = 0.10$ pH unit at pH = 7.6.

Then, we imaged by TPE 3T3 fibroblasts expressing untargeted E^2GFP, which distributes almost evenly between cytoplasm and nucleoplasm by passive diffusion.[22] Cells were imaged at the basal state (Fig. 2a) and under pro-apoptotic conditions upon H_2O_2 exposure (Fig. 2b). For each pixel the lifetime decay was converted into the corresponding phasor (Fig. 2c). Under physiological conditions, the average phasor of the main pixel cluster falls in the pH range of 7.0–7.25 (Fig. 2c and d) confirming the expected neutral pH of the fibroblasts in the resting state. Detailed analyses at the subcellular level indicated a rather homogeneous pH_i distribution ($\sigma = 0.25$ pH unit), independent of image zoom. Yet, the pixel pH distribution was slightly broader than those observed for images of cells clamped to a given pH ($\sigma = 0.17$ pH unit), witnessing the intrinsic pH variability of cells in the physiological state.[20]

These results compare well with previously reported data.[23] Indeed, cytoplasmic pH_i is strictly regulated by specific ioncoupled transporters[2] as well as aerobic and anaerobic metabolism,[24] and it typically lies within the 7.0–7.4 range; also, no pH_i gradients are observable between cytoplasm and nucleoplasm. Remarkably, the phasor plot allowed for the easy discrimination of pH-dependent E^2GFP fluorescence (phasors falling along the pH calibration line, Fig. 2c) and cell autofluorescence (phasors off the pH calibration line). After 5 minutes of incubation with 1.5% H_2O_2 in the culture medium, cells started to lower their pH in response to oxidative stress (Fig. 2c and e), the latter factor being a well-known trigger of cell apoptosis.[25] In keeping with the ongoing apoptotic process, the observed

acidification correlated with a significant cell shrinking, as visible from the comparison of intensity images (Fig. 2a and b). Again, autofluorescence phasors were easily distinguishable in the phasor plot, although they appeared slightly displaced with respect to the resting state (Fig. 2c and e).

The phasor analysis was then applied to identify pH of mitochondria. Measurements were performed by SPE on E^2GFP targeted to the mitochondrial matrix of HeLa cells by fusion with the subunit VIII of human cytochrome *c* oxidase (Fig. 2f and g). The mitochondrial matrix is known to possess a rather alkaline pH (>7.5), as the establishment of a proton gradient with cytoplasm is fundamental to the proton-transport process associated with ATP production by oxidative phosphorylation.[26] Consistently, the phasor plot yields pH = 8.0 for the mitochondrial matrix in resting cells (Fig. 2h and i). Oxidation-induced apoptosis appears to cause mitochondrial acidification.[25] We also tested the effect of 1.5% H_2O_2: the phasor plot clearly displays a marked decrease of mitochondrial pH down to 7.0 (Fig. 2g, h and j).

In conclusion, we demonstrated for the first time the application of phasor-based fluorescence lifetime imaging to intracellular pH determination under both resting and altered conditions. We took advantage of a genetically-encoded fluorescent protein whose physicochemical properties are strongly dependent on environmental pH on account of a proton dissociation equilibrium at the chromophore level. The versatility of our fluorescent probe allows cell imaging and pH determination both by single- and two-photon excitation.

Supplementary Material

Refer to Web version on PubMed Central for supplementary material.

Acknowledgments

This work was supported by ARIN S.p.A. - Naples (Italy), and FIRB project RBPR05JH2P by MIUR. M.A.D. and E.G. acknowledge support from NIH-P41-RR003155 and NIH-P50-GM076516. All authors acknowledge the help of Dr. Chiara Stringari for data analysis.

Notes and references

1. Putney LK, Barber DL. J Biol Chem. 2003; 278:44645. [PubMed: 12947095]
2. Hunte C, Screpanti E, Venturi M, Rimon A, Padan E, Michel H. Nature. 2005; 435:1197. [PubMed: 15988517]
3. Gruenberg J, Stenmark H. Nat Rev Mol Cell Biol. 2004; 5:317. [PubMed: 15071556]
4. Wakabayashi I, Poteser M, Groschner K. J Vasc Res. 2006; 43:238. [PubMed: 16449818]
5. Izumi H, Torigoe T, Ishiguchi H, Uramoto H, Yoshida Y, Tanabe M, Ise T, Murakami T, Yoshida T, Nomoto M, Kohno K. Cancer Treat Rev. 2003; 29:541. [PubMed: 14585264]
6. Carnell L, Moore HP. J Cell Biol. 1994; 127:693. [PubMed: 7962053]
7. Chesler M. Physiol Rev. 2003; 83:1183. [PubMed: 14506304]
8. Han J, Burgess K. Chem Rev. 2010; 110:2709. [PubMed: 19831417]
9. Bizzarri, R. Fluorescent Proteins II: Application of Fluorescent Protein Technology. Jung, G., editor. Springer-Verlag; Berlin: 2012.
10. Bizzarri R, Serresi M, Luin S, Beltram F. Anal Bioanal Chem. 2009; 393:1107. [PubMed: 19034433]
11. Voityuk AA, Michel-Beyerle ME, Rosch N. Chem Phys. 1998; 231:13.
12. Stoner-Ma D, Jaye AA, Ronayne KL, Nappa J, Meech SR, Tonge PJ. J Am Chem Soc. 2008; 130:1227. [PubMed: 18179211]
13. Suhling K, French PM, Phillips D. Photochem Photobiol Sci. 2005; 4:13. [PubMed: 15616687]

14. Liu Y, Kim HR, Heikal AA. J Phys Chem B. 2006; 110:24138. [PubMed: 17125385]
15. Jameson DM, Gratton E, Hall RD. Appl Spectrosc Rev. 1984; 20:55.
16. Digman MA, Caiolfa VR, Zamai M, Gratton E. Biophys J. 2008; 94:L14. [PubMed: 17981902]
17. Stringari C, Cinquin A, Cinquin O, Digman MA, Donovan PJ, Gratton E. Proc Natl Acad Sci U S A. 2011; 108:13582. [PubMed: 21808026]
18. Clayton AH, Hanley QS, Verveer PJ. J Microsc (Oxford, U K). 2004; 213:1.
19. Hirshfield KM, Toptygin D, Packard BS, Brand L. Anal Biochem. 1993; 209:209. [PubMed: 8470792]
20. Bizzarri R, Arcangeli C, Arosio D, Ricci F, Faraci P, Cardarelli F, Beltram F. Biophys J. 2006; 90:3300. [PubMed: 16603505]
21. Bizzarri R, Nifosi R, Abbruzzetti S, Rocchia W, Guidi S, Arosio D, Garau G, Campanini B, Grandi E, Ricci F, Viappiani C, Beltram F. Biochemistry. 2007; 46:5494. [PubMed: 17439158]
22. Cardarelli F, Bizzarri R, Serresi M, Albertazzi L, Beltram F. J Biol Chem. 2009; 284:36638. [PubMed: 19858191]
23. Lin HJ, Herman P, Lakowicz JR. Cytometry, Part A. 2003; 52:77.
24. Sun HY, Wang NP, Halkos ME, Kerendi F, Kin H, Wang RX, Guyton RA, Zhao ZQ. Eur J Pharmacol. 2004; 486:121. [PubMed: 14975701]
25. Lagadic-Gossmann D, Huc L, Lecureur V. Cell Death Differ. 2004; 11:953. [PubMed: 15195071]
26. Mitchell P, Moyle J. Nature. 1967; 213:137. [PubMed: 4291593]

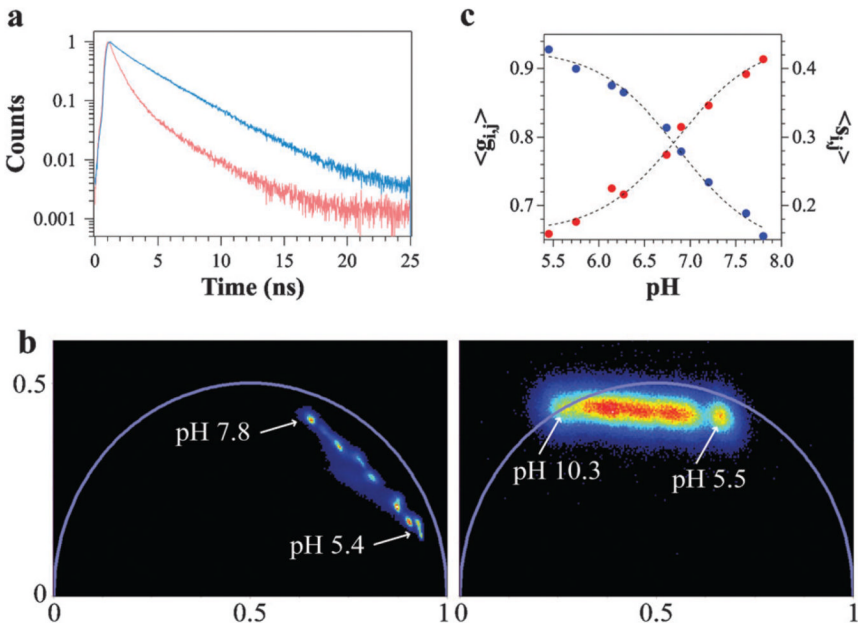

Fig. 1.

pH-dependent fluorescence lifetime features of E^2GFP upon single photon excitation (SPE) at 405 nm or two-photon excitation (TPE) at 800 nm. The collection range was 500–600 nm. (a) Normalized fluorescence decays *in vitro* for pH 5.49 (red) and pH 7.82 (blue) by SPE. (b) Phasor plots of universal pH calibration in CHO-K1 cells by SPE (left panel, modulation frequency 40 MHz) or *in vitro* by TPE (right panel, modulation frequency 80 MHz). (c) Plot of $\langle g_{i,j} \rangle$ (blue circles) and $\langle s_{i,j} \rangle$ (red circles) *vs.* pH for the calibration in CHO-K1 cells: fits to Henderson–Hasselbalch equation are displayed as dashed black curves.

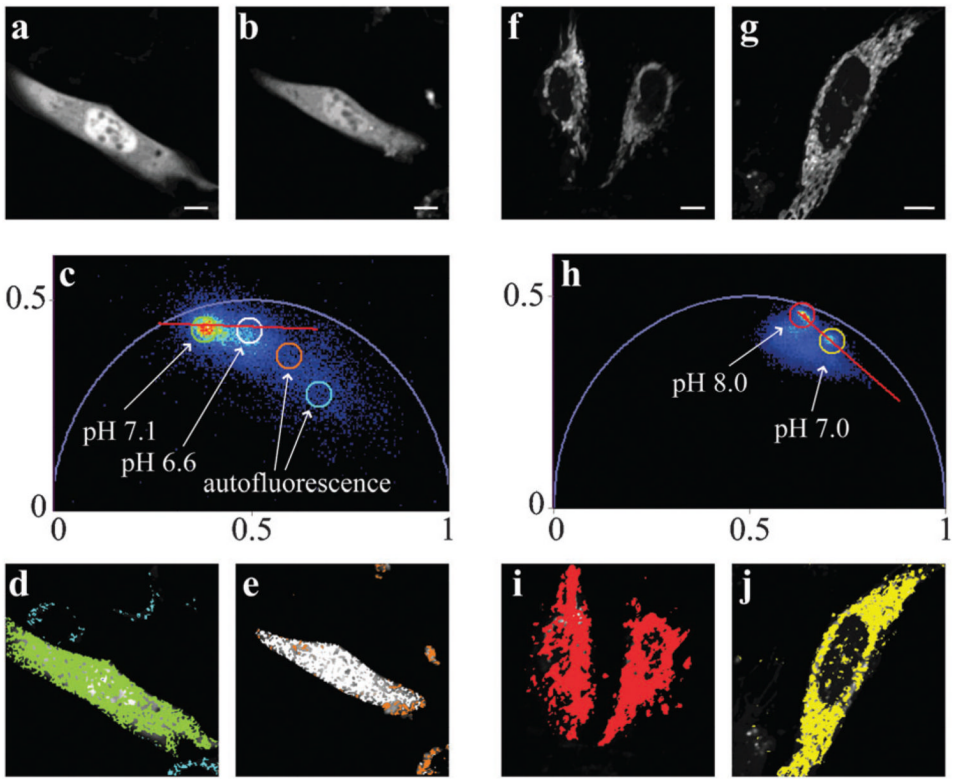

Fig. 2.

pH analysis of cells expressing E^2GFP in cytoplasm or mitochondria under resting conditions or pro-apoptotic oxidative stress (1.5% H_2O_2 for 5 min). (a and b) Cytoplasmic E^2GFP was imaged by TPE at 740 nm in a 3T3 fibroblast at rest (a) or under oxidative stress (b). (c) Phasor plots for images (a) and (b) together with pH calibration (red line); relevant pH and autofluorescence phasors are enclosed in colored circles. Note that the 800 nm TPE calibration applies also to measurements at 740 nm as demonstrated by average ΔpH = 0.06 at pH 7.0–7.2, which is consistent with the accuracy of pH measurements. (d) Same as image (a), but the pixels corresponding to pH 7.1 and autofluorescence are highlighted by the corresponding circle colors of the phasor plot. (e) Same as image (b), but the pixels corresponding to pH 6.6 and autofluorescence are highlighted by the corresponding circle colors of the phasor plot. (f and g) Mitochondrion-targeted E^2GFP was imaged by SPE at 405 nm in a HeLa cell at rest (f) or under pro-apoptotic oxidative stress (g). (h) Phasor plots for images (f) and (g) together with pH calibration (red line); relevant pH phasors are enclosed in colored circles. (i) Same as image (f), but the pixels corresponding to pH 8.0 are highlighted by the corresponding circle color of the phasor plot. (j) Same as image (g), but the pixels corresponding to pH 7.0 are highlighted by the corresponding circle color of the phasor plot. In all images, scale bar = 10 μm.

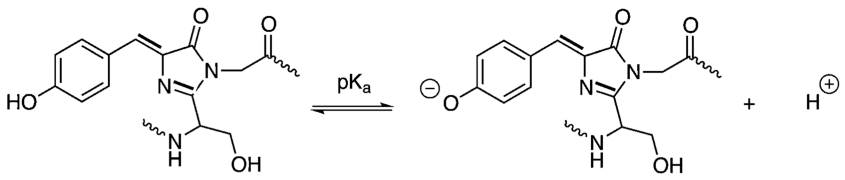

Protonated (neutral) state
λ_{ex} = 395-420 nm, λ_{em} = 475-510 nm

Deprotonated (anionic) state
λ_{ex} = 475-525 nm, λ_{em} = 510-530 nm

Chart 1.